DSCC2014-6149

DESIGN OF RIGHTMOST EIGENVALUES USING DISTRIBUTED DELAY

Feng Wei
Department of Mathematics
University of Michigan
Ann Arbor, Michigan 48109
Email: weifeng@umich.edu

Gábor Orosz[*]
Dept. of Mechanical Engineering
University of Michigan
Ann Arbor, Michigan 48109
Email: orosz@umich.edu

A. Galip Ulsoy
Dept. of Mechanical Engineering
University of Michigan
Ann Arbor, Michigan 48109
Email: ulsoy@umich.edu

ABSTRACT

This paper considers the problem of designing the rightmost eigenvalues of linear scalar distributed delay systems using two different but complementary methods: generalized stability charts and matrix Lambert W functions. The generalized stability charts are based on generalized Hopf and fold curves that provide important insight into the problem, but the geometry of the curves may become complicated for certain delay distributions. The Lambert W function approach can be applied to general delay distributions, but requires numerical solutions which can suffer from convergence problems. We present simple examples for both approaches.

1 INTRODUCTION

In many engineering applications one tries to achieve a desired dynamic behavior, e.g., settling time in the vicinity of an equilibrium, by designing the eigenvalues of the corresponding linear systems. Examples include, vibration absorbers [1,2], machining processes [3,4], vehicle steering [5,6], and connected vehicles [7,8]. Of special interest are the rightmost or leading eigenvalues. These determine the linear stability of the equilibrium and, for a stable system, they correspond to solutions with the slowest decay [9]. Thus, the desired dynamic behavior may be achieved by selecting the system parameters (including control gains) so that the rightmost eigenvalues are placed appropriately as demonstrated in the recent papers [10–12].

However, systems with time delay exhibit an infinite spectrum, which makes eigenvalue placement very challenging, even

though the dynamic response is still dominated by the rightmost eigenvalues [13–15]. Here, apart from designing the system parameters, one may also tune the delays in order to place the eigenvalues appropriately [16, 17], though limitations may arise due to the achievable minimal value of the delay. Such limitations may be compensated for in systems with distributed delays where apart from system parameters one may design the delay distribution [18,19]. Practical examples include the design of the cutting profile of helical milling tools in machining [3, 4], where the delay distributions originate from spatial force distributions. Similar ideas may also be used when designing transmission protocols for vehicle-to-vehicle communication in connected vehicle systems [7, 8], where the delay distributions originate from stochastic delay variations.

In this paper, we investigate the problem of spectrum design for the rightmost eigenvalues of a linear scalar system with distributed delay while considering constant delay distribution. A treatment of more general distributions can be found in [20]. We apply two complementary approaches: the bifurcation theory approach and the Lambert W function approach. In the bifurcation theory approach, we extend the idea of a stability chart [21, 22] for a general case when the leading eigenvalues have non-zero real part. That is we transform the design problem to finding the locations of generalized Hopf and fold bifurcations in parameter space. Design limitations are also investigated using numerical continuation. As for the Lambert W function approach, we reformulate the problem as a special case of a delayed system with a single constant delay and then apply the matrix Lambert W function method [15]. Here, we exploit the structure of the arising system matrices to accelerate the numerical computation.

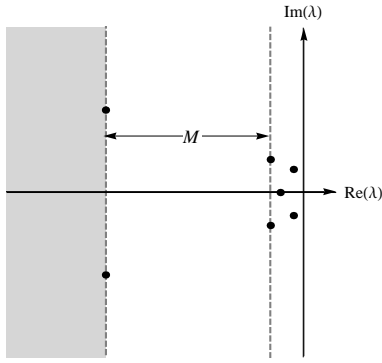[*]Address all correspondence to this author.

FIGURE 1. An illustration of the spectrum design where the five rightmost eigenvalues are placed and a spectral gap of size M is created.

We also highlight some numerical issues arising due to multiple eigenvalues associated with this problem.

We present scenarios where the real part of the leading eigenvalues is negative (stable systems) and also when it is positive (unstable systems). The former case is related to robust stability [21], which is important in many engineering applications. The latter case is also relevant in that unstable systems can exhibit high performance when operated by skilled operators or are regulated by well-designed controllers. Examples include, nuclear reactors, steering systems, and aircrafts with forward swept wings [23].

2 PROBLEM FORMULATION

Consider the following scalar linear differential equation with distributed delay:

$$\frac{\mathrm{d}}{\mathrm{d}\tau}x(\tau) = \alpha x(\tau) + \beta \int_{-h}^{0} w(\xi)x(\tau+\xi)\mathrm{d}\xi\,, \qquad (1)$$

where the initial condition is given by $x(\tau) = \phi(\tau),\ -h \le \tau \le 0$, and the delay distribution satisfies $\int_{-h}^{0} w(\xi)\mathrm{d}\xi = 1$. We know that the eigenvalues give an infinite spectrum $\{\lambda_i\}_{i=1}^{\infty}$ and that the solution of (1) can be written as $x(\tau) = \sum_{i=1}^{\infty} C_i \mathrm{e}^{\lambda_i \tau}$, where the coefficients C_i depend on the initial condition $\phi(\tau)$ (often called preshape function) [15, 22]. The rightmost eigenvalues with the largest real part dominate the system dynamics. Thus, placing these appropriately and creating a spectral gap between these and the rest of the eigenvalues allows us to design a system with desired temporal behavior.

To place the rightmost p eigenvalues of (1) at $\lambda_1,\ldots,\lambda_p$, we need to select the appropriate parameter values α, β and the weight function $w(\xi)$. If we want the rightmost p eigenvalues to dominate the dynamics, we also need to create a spectral gap

so that $\mathrm{Re}(\lambda_j) \le \mathrm{Re}(\lambda_i) - M, 1 \le i \le p < j$, where M is a positive real number. Such a setup is illustrated in Fig. 1, where we specified the rightmost five eigenvalues as well as the spectral gap of size M in the complex plane, i.e., all other eigenvalues are located in the shaded region. We remark that this is equivalent to designing the rightmost $p+1$ or $p+2$ eigenvalues such that the difference between the real parts of the left-most designed eigenvalues provides the spectral gap; see Fig. 1. In some applications, we only care about the real part of the eigenvalues, and can, thus, formulate a less restrictive problem where only $\mathrm{Re}(\lambda_i)$, $i = 1,\ldots,p+1$ are assigned.

Rescaling time as $\tau = ht, \xi = h\theta$ allows us to write (1) into the form

$$\dot{x}(t) = ax(t) + b\int_{-1}^{0} w(\theta)x(t+\theta)\,\mathrm{d}\theta\,, \qquad (2)$$

where the dot stands for differentiation with respect to the rescaled time t and we have the design parameters

$$a = h\alpha\,, \quad b = h^2\beta\,. \qquad (3)$$

where the maximum delay h appears as as a scaling factor.

In this paper, we focus on the special case of $w(\theta) \equiv 1$, which means that (2) simplifies to

$$\dot{x}(t) = ax(t) + b\int_{-1}^{0} x(t+\theta)\mathrm{d}\theta\,. \qquad (4)$$

More general weight functions are considered in [20]. Substituting the trial solution $x(t) = \mathrm{e}^{\lambda t}$ results in the characteristic equation

$$D(\lambda) = \lambda - a - b\frac{1-\mathrm{e}^{-\lambda}}{\lambda} = 0\,, \qquad (5)$$

which has infinitely many solutions for the eigenvalues λ. Note that one may define an operator which possesses these eigenvalues and serves as the infinitesimal generator for (4) in the infinite dimensional space of continuous functions on $[-1,0]$; see [21, 22].

3 BIFURCATION THEORY APPROACH

When system parameters are varied the trivial solution $x(t) \equiv 0$ of a linear system can lose stability in two possible ways. Either a real eigenvalue moves through zero to the right half complex plane (leading to non-oscillatory stability loss), or a pair of complex conjugate eigenvalues cross the imaginary axis

from left to right (leading to oscillatory stability loss where the frequency is given by the imaginary part of those eigenvalues). In the corresponding nonlinear system, fold and Hopf bifurcations may occur. In the parameter plane, stable and unstable domains are separated by stability curves, which are often categorized as fold and Hopf curves. We adopt this terminology here even though we do not investigate nonlinear effects. Moreover, we define generalized stability curves (i.e., generalized fold and Hopf curves) that correspond to eigenvalues that cross a given vertical line in the complex plane. Note that these are not related to bifurcations in the corresponding nonlinear system and only make sense at the linear level. These generalized curves allow us to locate parameter values that correspond to given eigenvalue configurations for the leading eigenvalues.

Substituting $\lambda = \gamma \pm i\omega$ into (5), separating real, and imaginary parts and assuming $\omega > 0$, we obtain

$$a = \gamma + \frac{\gamma - e^{-\gamma}(\gamma \cos \omega - \omega \sin \omega)}{1 - e^{-\gamma}(\omega \cos \omega + \gamma \sin \omega)/\omega},$$
$$b = -\frac{\gamma^2 + \omega^2}{1 - e^{-\gamma}(\omega \cos \omega + \gamma \sin \omega)/\omega}, \tag{6}$$

which describe the generalized Hopf curves in the (a, b)-plane in parameterized form. For $\omega = 0$, Eq. (5) results in

$$b = \frac{\gamma}{1 - e^{-\gamma}}(\gamma - a), \tag{7}$$

and the corresponding straight line is the generalized fold curve in the (a, b)-plane. Indeed, the curves given by (6) and (7) change with γ. For $\gamma = 0$ they are the stability boundaries, while for $\gamma \neq 0$ they produce diagrams which we refer as generalized stability charts. We remark that $\gamma < 0$ corresponds to robust stability [21], while $\gamma > 0$ corresponds to unstable design.

Fig. 2 shows generalized stability charts for different values of γ. Straight lines and curves correspond to generalized fold and Hopf curves, respectively. The numbers indicate how many eigenvalues with real part larger than γ are in that region. These can be determined by calculating the eigenvalues numerically at a chosen point within a chosen domain and then counting the number crossing eigenvalues when moving from one domain to another; see [20] for more details. The shaded regions (bounded by solid curves) are the generalized stability regions. The arrows show how the frequency ω increases along the Hopf curves and the values of ω corresponding to $a, b \to \pm\infty$ are also indicated. The left panel in Fig. 2 shows the case where $\gamma = 0$, which is the stability chart. When $\omega \to 2k\pi, k = 1, 2, \ldots$ the parameters a, b go to infinity because the denominator

$$d(\gamma, \omega) = 1 - e^{-\gamma}(\omega \cos \omega - \gamma \sin \omega)/\omega, \tag{8}$$

in (6) goes to zero. In the middle panel of Fig. 2 we have $\gamma = -0.5$. The diagram looks similar to the $\gamma = 0$ case, since a, b still go to infinity at some finite values of ω. However, some Hopf curves appear in the upper half plane and generate regions with odd numbers of "unstable" eigenvalues. Also, the Hopf curves show asymptotic behavior when $\omega \to \omega_k, k = 1, 2, \ldots$ (but $\omega_k \neq k\pi$), and the curves are hyperbolic (while for $\gamma = 0$ they were parabolic). The right panel in Fig. 2 depicts the generalized stability chart for $\gamma = 0.5$ which looks quite different from the other panels: the Hopf curve does not go to infinity at finite values of ω, but intersect itself and creates loops.

To better understand the difference between the three cases above, we plot the denominator (8) as a function of the frequency ω for different values of γ in Fig. 3. For $\gamma = 0$ (red dashed curve) the denominator becomes zero at $\omega = 2k\pi, k = 1, 2, \ldots$; cf. the left panel of Fig. 2. For $\gamma = -0.5$ the blue solid curve intersects the horizontal axis at $\omega = \omega_k, k = 1, 2, \ldots$. Along the intervals $\omega \in [\omega_k, \omega_{k+1}]$ where k is odd, the curve is negative and this correspond to the generalized Hopf curves above the horizontal axis in the middle panel of Fig. 2. Finally, for $\gamma = 0.5$ (green dotted curve) the denominator is positive for all ω values and the corresponding generalized stability curve does not go to infinity for finite values of ω; cf. the right panel of Fig. 2.

By tuning the parameters a, b there are several leading eigenvalue configurations that can be designed:

1. Two real eigenvalues (e.g., $\lambda_1 = -1$ and $\lambda_2 = -3$);
2. One real eigenvalue and real part of a pair of two complex conjugate eigenvalues (e.g., $\lambda_1 = -1$ and $\lambda_{2,3} = -3 \pm i\omega$);
3. Real parts of two pairs of complex conjugate eigenvalues (e.g., $\lambda_{1,2} = -1 \pm i\omega$ and $\lambda_{3,4} = -3 \pm i\tilde{\omega}$);
4. One pair of complex conjugate eigenvalues (e.g., $\lambda_{1,2} = -0.5 \pm i3$);

We will show below an example for each case.

3.1 Designing two real eigenvalues

One way to design a spectral gap is to design two real eigenvalues. To illustrate this, Fig. 4 shows the generalized stability boundaries for $\gamma_1 = -1$ (blue curves) and $\gamma_2 = -3$ (red curves). The blue and red shaded regions correspond to eigenvalues that have real part less than γ_1 and γ_2, respectively. The number of "unstable" eigenvalues are indicated in each region for both cases: the first element of the pair gives how many eigenvalues have real part larger then γ_1 while the second element shows this for γ_2. By substituting γ_1 and γ_2 into (7) one may find that the corresponding generalized fold curves intersect at

$$a_{\text{ff}} = \gamma_1 + \frac{M(1 - e^{\gamma_1})(\gamma_1 - M)}{M(1 - e^{\gamma_1}) - \gamma_1(1 - e^M)},$$
$$b_{\text{ff}} = \frac{\gamma_1 M e^{\gamma_1}(\gamma_1 - M)}{M(1 - e^{\gamma_1}) - \gamma_1(1 - e^M)}, \tag{9}$$
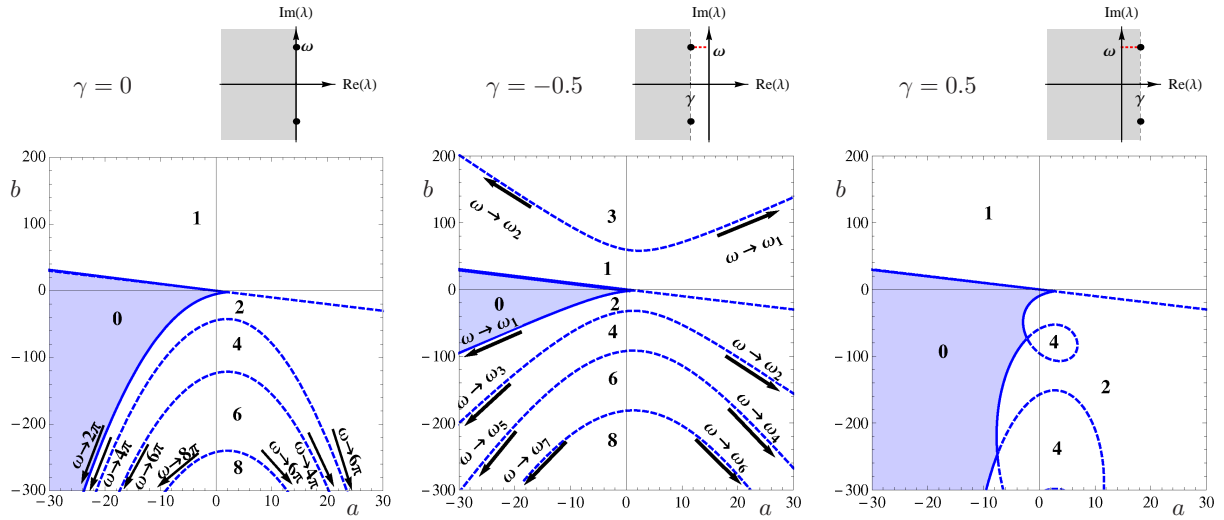
FIGURE 2. Generalized stability charts for different values of the real part γ as indicated above. In the shaded regions (bounded by solid curves) all eigenvalues have real part smaller than γ. In each region the number of "unstable" eigenvalues (with real part larger than γ) are indicated.

where $M = \gamma_1 - \gamma_2$ is the size of the spectral gap. In particular, for $\gamma_1 = -1$ and $\gamma_2 = -3$ we obtain $(a,b) \approx (-0.26, -0.43)$, which is denoted by D_1 in Fig. 4 and the corresponding eigenvalue configuration is shown at the bottom. Since D_1 is at the boundary of regions $(1,\cdot),(0,\cdot)$, the rightmost eigenvalue is $\lambda_1 = \gamma_1$. Similarly, the second eigenvalue is $\lambda_2 = \gamma_2$, since D_1 is at the boundary of regions $(\cdot,1),(\cdot,2)$.

The question arises whether there is a limitation in the design for two real eigenvalues. Due to (7), the two fold curves with different γ are not parallel, so they always intersect at (9). Moreover, the intersection always produces the desired eigenvalue configuration $\gamma_1 > \gamma_2$, i.e., the solid segment of the γ_1 line intersects dashed segment of the γ_2, because other cases contradict the fact that γ_1 corresponds to the leading eigenvalue followed by the eigenvalue at γ_2.

3.2 Designing one real eigenvalue and the real part of a pair of complex conjugate eigenvalues

Alternatively, one can design one real eigenvalue and a pair of complex conjugate eigenvalues with a fixed real part, that is, consider the rightmost three eigenvalues to be $\lambda_1 = \gamma_1$ and $\lambda_{2,3} = \gamma_2 \pm i\omega$ where ω is arbitrary. As shown in Fig. 4, the fold curve for $\gamma_1 = -1$ and a Hopf curve for $\gamma_2 = -3$ intersect at $(a,b) \approx (-4.97, 2.31)$ which is denoted by D_2 and corresponds to the eigenvalue configuration displayed at the bottom. Since D_2 is at the boundary of regions $(1,\cdot),(0,\cdot)$, the rightmost eigenvalue is at $\lambda_1 = \gamma_1$. The second and third eigenvalues are at $\lambda_{2,3} = \gamma_2 \pm i\omega$, since D_2 is also at the boundary of regions $(\cdot,1),(\cdot,3)$.

The limitations of this design may be of interest. Substituting γ_1 into (7) and γ_2 into (6) and eliminating a and b one may

derive

$$
\begin{aligned}
&-\omega\big((\gamma_1-\gamma_2)^2+\omega^2\big)+e^{-\gamma_1}\omega(\gamma_2^2+\omega^2)+e^{-\gamma_2}\gamma_1 \\
&\times\Big(\big(\gamma_2(\gamma_1-\gamma_2)+\omega^2\big)\sin\omega+(\gamma_1-2\gamma_2)\omega\cos\omega\Big)=0.
\end{aligned}
\tag{10}
$$

By plotting the corresponding surface in the three dimensional space $(\gamma_1, \gamma_2, \omega)$, one can show that it is contained in the domain $\gamma_2 < 0$, $\gamma_2 < \gamma_1$. This indicates that it is not possible to place the complex conjugate eigenvalues to the right of the real eigenvalue. This can also be observed in Fig. 4 as the fold curve that belongs to $\gamma_2 = -3$ does not intersect Hopf curves belonging to $\gamma_1 = -1$.

3.3 Designing the real parts of two pairs of complex conjugate eigenvalues

Based on the above argument, when the rightmost eigenvalues are given by a complex conjugate pair, a spectral gap can only be provided if these are followed by another pair of complex conjugate eigenvalues. Suppose our desired rightmost four eigenvalues are $\lambda_{1,2} = \gamma_1 \pm i\omega$, $\lambda_{3,4} = \gamma_2 \pm i\tilde{\omega}$, where $\omega, \tilde{\omega}$ are arbitrary. In Fig. 4, a blue Hopf curve for $\gamma_1 = -1$ and a red Hopf curve for $\gamma_2 = -3$ intersect at $(a,b) \approx (-3.20, -4.16)$ which is denoted by D_3 and the corresponding eigenvalue configuration is shown at the bottom. Thus, the rightmost eigenvalues are $\lambda_{1,2} = \gamma_1 \pm i\omega$, since D_3 is at the boundary of regions $(2,\cdot),(0,\cdot)$. Similarly, the second pair of eigenvalues is $\lambda_{3,4} = \gamma_2 \pm i\tilde{\omega}$, since D_3 is at the boundary of regions $(\cdot,2),(\cdot,4)$. One can also investigate the limitation of spectrum design for this case, but we leave that as a problem for future research.
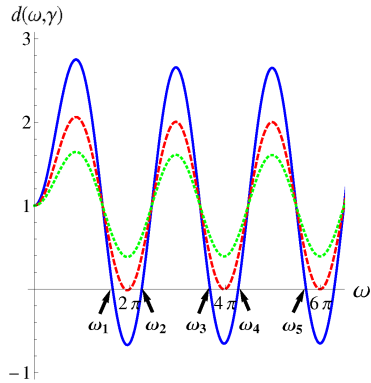
4

FIGURE 3. The denominator (8) for different values of the real part: $\gamma = 0$ — red dashed, $\gamma = -0.5$ — blue solid, $\gamma = 0.5$ — green dotted.
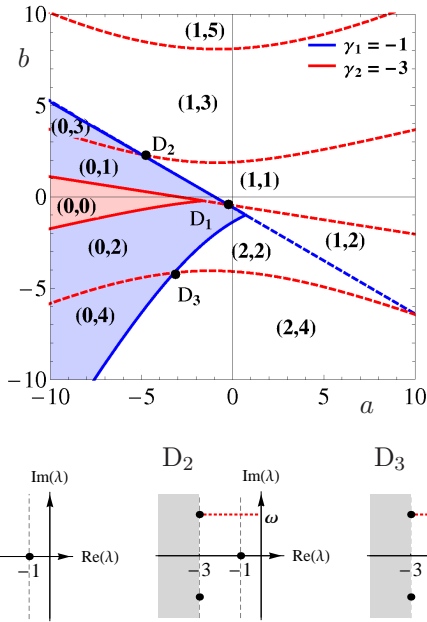

FIGURE 4. Generalized stability charts for $\gamma_1 = -1$ (blue) and $\gamma_2 = -3$ (red). The first and second elements of the number pairs indicate how many eigenvalues have real part larger than -1 and -3, respectively. The intersections marked as D_1, D_2, D_3 correspond to the designed eigenvalue configurations shown at the bottom where the frequencies ω and $\tilde{\omega}$ are not specified.

3.4 Designing a pair of complex conjugate eigenvalues

Finally, we can design the rightmost complex conjugate pair $\lambda_{1,2} = \gamma \pm i\omega$ without specifying a spectral gap , which is equivalent to saying that there is a generalized Hopf type of stability loss at γ with given frequency ω. This corresponds to a point
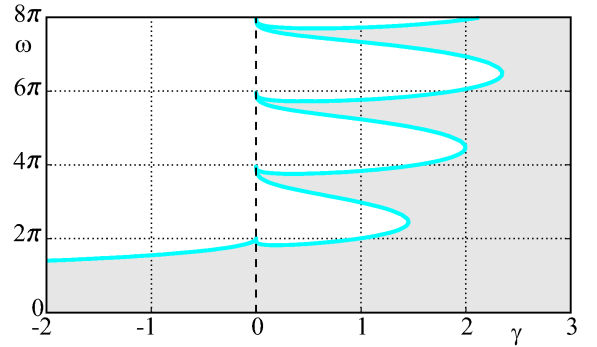

FIGURE 5. Available region for the real and imaginary parts of the designed eigenvalues.

on a "primary" generalized Hopf curve, i.e., on a solid curve in Fig. 2 constituting a boundary between regions with 0 and 2 "unstable" eigenvalues. (Dashed curves separate regions with higher numbers of eigenvalues.)

In this case, one is interested in the limitations in γ and ω. For $\gamma \leq 0$ the primary Hopf curve corresponds to the frequency domain $\omega \in [0, \omega_1]$ where ω_1 is the minimum positive frequency for which $d(\gamma, \omega) = 0$, cf. (8) and Fig. 3. However, the limitations for $\gamma > 0$ are harder to determine due to the self intersections of the Hopf curve that correspond to having two different frequencies $\omega_1 \neq \omega_2$ for fixed γ; cf. the right panel of Fig. 2. Consider (6) and solve the system

$$
\begin{aligned}
0 &= a(\omega_1, \gamma) - a(\omega_2, \gamma), \\
0 &= b(\omega_1, \gamma) - b(\omega_2, \gamma),
\end{aligned}
\tag{11}
$$

for ω_1, ω_2 which is equivalent to finding the equilibria of the related mock differential equation

$$
\begin{aligned}
\dot{\omega}_1 &= a(\omega_1, \gamma) - a(\omega_2, \gamma), \\
\dot{\omega}_2 &= b(\omega_1, \gamma) - b(\omega_2, \gamma),
\end{aligned}
\tag{12}
$$

where γ is considered as a parameter. Indeed, when γ is varied, the equilibrium changes. We use numerical continuation [24], in particular the package DDE-BIFTOOL [25], to continue the solution while changing γ and the boundary is shown in the complex plane in Fig. 5. Here shading denotes the region in the complex plane where eigenvalues can be placed.

Finally, we discuss the special case when $\omega = 0$ which yields the leading eigenvalue $\lambda_{1,2} = \gamma$ with multiplicity two. This can also be obtained by setting $\gamma_1 = \gamma_2 = \gamma$ when considering two real leading eigenvalues as was discussed in Sec. 3.1. To obtain the corresponding parameter values one needs to solve $D(\gamma) = 0$ and $\partial D(\gamma)/\partial \gamma = 0$ for a and b. Thus, the characteristic equation

(5) leads to the parametric curve

$$a = \gamma\left(2 + \frac{\gamma}{e^\gamma - 1 - \gamma}\right),$$
$$b = -\frac{\gamma^2 e^\gamma}{e^\gamma - 1 - \gamma}, \tag{13}$$

that is shown as a green curve in Fig. 7. The green dot indicates where $\gamma = 0$ and γ increases from left to right along the curve as indicated by arrows. On one hand, one may use the left section of the curve to design systems with "critical damping". On the other hand, multiplicity may lead to convergence problems for numerical methods as will be discussed in Sec. 4.1.

4 LAMBERT W FUNCTION METHOD

The scalar distributed delay system (4) can be converted into a system of two scalar variables with discrete delay. Then the assignment of its eigenvalues can readily be handled by the matrix Lambert W function method [14], using the Lambert W toolbox [26]. The advantage of the Lambert W function approach is that the real part of the eigenvalues follows the order of the branch number [15]. This allows one to focus on a few rightmost eigenvalues as is our goal here.

Multiplying (5) with λ yields

$$D(\lambda) = \lambda^2 - a\lambda - b(1 - e^{-\lambda}), \tag{14}$$

which is the characteristic equation of the 2-nd order system

$$\ddot{x}(t) = a\dot{x}(t) + b(x(t) - x(t-1)). \tag{15}$$

Note that when multiplying by λ, we introduce a zero eigenvalue into the spectrum. We refer to this as an "intrinsic" zero eigenvalue.

Let us define the vector

$$\mathbf{x}(t) = \begin{bmatrix} x(t) \\ \dot{x}(t) \end{bmatrix}, \tag{16}$$

then (15) is equivalent to the system

$$\dot{\mathbf{x}}(t) = \mathbf{A}\mathbf{x}(t) + \mathbf{A}_{\mathrm{d}}\mathbf{x}(t-1), \tag{17}$$

where the matrices $\mathbf{A}, \mathbf{A}_{\mathrm{d}} \in \mathbb{R}^{2 \times 2}$ are defined as

$$\mathbf{A} = \begin{bmatrix} 0 & 1 \\ b & a \end{bmatrix}, \quad \mathbf{A}_{\mathrm{d}} = \begin{bmatrix} 0 & 0 \\ -b & 0 \end{bmatrix}. \tag{18}$$

We need to select the parameters a, b in the matrices $\mathbf{A}, \mathbf{A}_{\mathrm{d}}$ to get the desired spectrum (plus one zero intrinsic eigenvalue).

To compute the eigenvalues of (17) using the Lambert W function approach [14, 15]. We need to solve the following equations

$$\mathbf{A}_{\mathrm{d}} = \mathbf{W}_{\mathbf{k}}(\mathbf{A}_{\mathrm{d}}\mathbf{Q}_{\mathbf{k}}) e^{\mathbf{W}_{\mathbf{k}}(\mathbf{A}_{\mathrm{d}}\mathbf{Q}_{\mathbf{k}})+\mathbf{A}},$$
$$\mathbf{S}_{\mathbf{k}} = \mathbf{W}_{\mathbf{k}}(\mathbf{A}_{\mathrm{d}}\mathbf{Q}_{\mathbf{k}}) + \mathbf{A}, \tag{19}$$

where $\mathbf{W}_{\mathbf{k}}$ is the matrix Lambert W function and the vector $\mathbf{k} = [\, k_1, \ k_2 \,]$ is the (vector-valued) branch number so that $k_i \in \{0, \pm 1, \pm 2, \ldots\}$. Solving the first equation for $\mathbf{Q}_{\mathbf{k}}$, one can use the second equation to obtain $\mathbf{S}_{\mathbf{k}}$ and the eigenvalues of $\mathbf{S}_{\mathbf{k}}$ give the eigenvalues of (14). In general, when considering $\mathbf{k} = [\, 0, \ 0 \,]$ the corresponding $\mathbf{S}_{\mathbf{k}}$ possesses the two leading eigenvalues, while considering $\mathbf{k} = [\, +1, \ +1 \,]$ and $\mathbf{k} = [\, -1, \ -1 \,]$ we can cover the following two eigenvalues and so on. However, since one eigenvalue of the matrix $\mathbf{A}_{\mathrm{d}}\mathbf{Q}_{\mathbf{k}}$ is zero, it is necessary to use hybrid branches where $k_i \neq k_j$. In this case one needs to consider three different $\mathbf{k}$ vectors that include all $k_i \in \{0, \pm 1\}$ in order to ensure that we cover the two leading eigenvalues [15].

Here we combine the eigenvalue calculations [26] with a root finding algorithm. This way the iterations converge to the parameter values that ensure the required eigenvalue configuration. However, these numerical iterations may be time consuming and the speed of convergence can depend on the selected initial value of $\mathbf{Q}_{\mathbf{k}}$.

Let us define the notation

$$\mathbf{Q}_{\mathbf{k}} = \begin{bmatrix} q_{11}^{\mathbf{k}} & q_{12}^{\mathbf{k}} \\ q_{21}^{\mathbf{k}} & q_{22}^{\mathbf{k}} \end{bmatrix}, \tag{20}$$

where the vector-values index $\mathbf{k}$ is switched to a superscript to simplify the notation. Notice that if we define

$$\mathbf{Q}_{\mathbf{k}} = \begin{bmatrix} q_{11}^{\mathbf{k}} & q_{12}^{\mathbf{k}} \\ 0 & 0 \end{bmatrix}, \tag{21}$$

then, due to the sparse structure of $\mathbf{A}_{\mathrm{d}}$ in (18), both (20) and (21) yields

$$\mathbf{A}_{\mathrm{d}}\mathbf{Q}_{\mathbf{k}} = \begin{bmatrix} 0 & 0 \\ -bq_{11}^{\mathbf{k}} & -bq_{12}^{\mathbf{k}} \end{bmatrix}. \tag{22}$$

This implies that there always exists a solution of $\mathbf{Q}_{\mathbf{k}}$ in the form of (21), i.e., we can assume an initial matrix $\mathbf{Q}_{\mathbf{k}}$ with the above sparse structure which reduces the computation time significantly. As shown in the Appendix, using hybrid branches
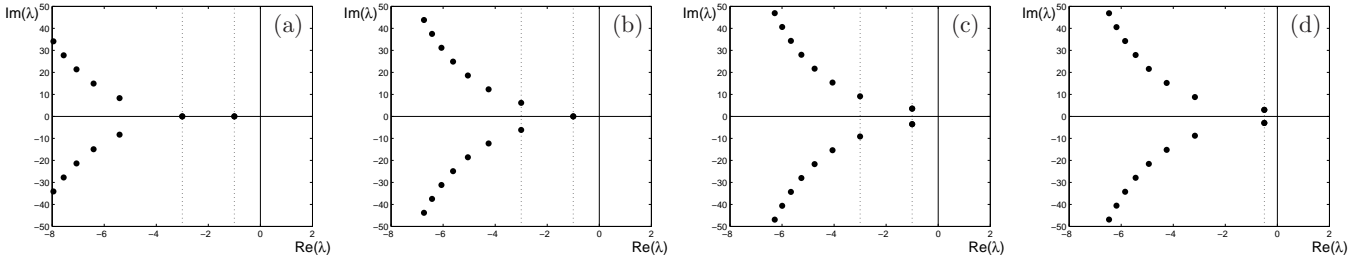
FIGURE 6. Eigenvalue configurations designed using the Lambert W approach. Panels (a), (b) and (c) correspond to the points D_1, D_2 and D_3 in Fig. 4. For panel (d) the real and imaginary parts of only the leading eigenvalues are designed. The corresponding numerical values are shown in Table 1.

with branch numbers $\mathbf{k} = [\, 0,\, k\,]$ we obtain

$$\mathbf{W_k}(\mathbf{A_d Q_k}) = \begin{bmatrix} 0 & 0 \\ W_k(-bq_{12}^{\mathbf{k}})q_{11}^{\mathbf{k}}/q_{12}^{\mathbf{k}} & W_k(-bq_{12}^{\mathbf{k}}) \end{bmatrix}. \qquad (23)$$

Substituting (21,22,23) into the first equation of (19) results in

$$\begin{bmatrix} 0 & 0 \\ -b & 0 \end{bmatrix} = \begin{bmatrix} 0 & 0 \\ W_k(-bq_{12}^{\mathbf{k}})q_{11}^{\mathbf{k}}/q_{12}^{\mathbf{k}} & W_k(-bq_{12}^{\mathbf{k}}) \end{bmatrix}$$
$$\times \exp\left(\begin{bmatrix} 0 & 1 \\ W_k(-bq_{12}^{\mathbf{k}})q_{11}^{\mathbf{k}}/q_{12}^{\mathbf{k}} + b & W_k(-bq_{12}^{\mathbf{k}}) + a \end{bmatrix} \right). \qquad (24)$$

After calculating the matrix exponential on the right hand side we obtain two coupled scalar equations that can be numerically solved for $q_{11}^{\mathbf{k}}$ and $q_{12}^{\mathbf{k}}$. This way the computational demand can be reduced significantly compared to using the standard matrix Lambert W approach. For example, if we select $a \in [-2,0]$ and $b = 1$ in (17,18) it takes approximately 100 seconds (on a standard desktop computer) to compute the eigenvalues for branches $0, \pm 1, \pm 2$ using the standard matrix Lambert W approach. Once we exploit the presence of zeros in $\mathbf{Q_k}$, it only takes about 1 to 2 seconds. Note that in order to reproduce the two leading eigenvalues it is adequate to consider the hybrid branches with branch numbers $[\, 0,\, 0\,]$, $[\, 0,\, +1\,]$, $[\, 0,\, -1\,]$ but we will show a more complete eigenvalue picture when presenting the results. We remark that each hybrid branch also reproduces the intrinsic zero eigenvalue but since this does not have physical meaning we do not show this on the figures.

Figure 6(a), (b) and (c) show the eigenvalues corresponding to the cases D_1, D_2 and D_3 in Fig. 4, respectively. The numerical values of the designed eigenvalues and the corresponding parameters are given in Table 1. We remark that in cases (b) and (c), only the real parts of the eigenvalues are given while the imaginary parts are obtained through the design procedure. Figure 6(d)

	eigenvalues	parameters
(a)	$\lambda_1 = -1$, $\lambda_2 = -3$	$(a,b) = (-0.26, -0.43)$
(b)	$\lambda_1 = -1$, $\lambda_{2,3} = -3 \pm \mathrm{i}6.15$	$(a,b) = (-4.97, 2.31)$
(c)	$\lambda_{1,2} = -1 \pm \mathrm{i}3.53$, $\lambda_{3,4} = -3 \pm \mathrm{i}9.11$	$(a,b) = (-3.20, -4.16)$
(d)	$\lambda_{1,2} = -0.5 \pm \mathrm{i}3$	$(a,b) = (-0.73, -3.46)$

TABLE 1. Numerical values corresponding to the panels of Fig. 6. Note that in cases (b) and (c) only the real parts of the eigenvalues are designed.

shows the case when the leading complex conjugate pair is designed so that both the real and imaginary parts are prescribed; see Table 1 for the numerical values of eigenvalues and parameters. In case (d), the design can be achieved since the desired eigenvalues lie in the shaded domain in Fig. 5.

4.1 Numerical issues

Although the Lambert W function is useful for computing the spectrum of a distributed delay system, there are certain values of parameters for which we run into numerical convergence problems. To characterize these areas (for the case of constant weight function) in the parameter plane we randomly select parameters in the range $(a,b) \in (-10, 10)$ and then randomly select the initial values for $q_{11}^{\mathbf{k}}$ and $q_{12}^{\mathbf{k}}$ in (24) with real and imaginary parts contained by the interval $(-10, 10)$. If the iterations converge, we plot a gray asterisk in the (a,b)-plane as shown in Fig. 7. Notice that no convergence were achieved in a strip and in the left part of the selected regime.

Note that the hybrid branch approach can only be applied when the Jordan form of $\mathbf{A_d Q_k}$ is diagonal (cf. Appendix) which may lead to convergence problems when the leading eigenvalues have multiplicity greater than one. To illustrate this we added the stability curves (6,7) for $\gamma = 0$ to Fig. 7 (cf. the left panel of Fig. 2). Along the straight fold line the eigenvalue 0 has multiplicity two due to the intrinsic zero eigenvalue generated when
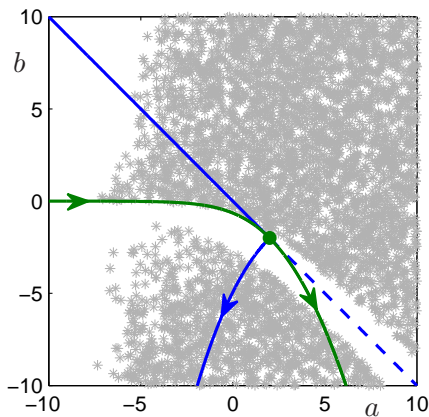
7

FIGURE 7. Convergence regions and multiplicities in the parameter plane. The gray area indicates where Lambert W function approach converges. The blue curves correspond to stability boundaries given by (6,7) for $\gamma = 0$ where the arrow indicates the increase of ω along the Hopf curve. The green curve is given by (13) and it shows the location where the systems has a leading eigenvalue of multiplicity two. The arrows show increase of γ and the green dot indicates $\gamma = 0$.

rewriting the system into vectorial form. Moreover, the green curve, given by (13), corresponds to the case where the lead eigenvalue is real and has multiplicity two (while the intrinsic zero eigenvalue still exists). At the intersection of the curves (indicated by green dot) we have a zero eigenvalue of multiplicity three. Figure 7 demonstrates that sections of these curves coincide with the strip where the Lambert W approach does not converge. However, it is not a one-to-one correspondence. Understanding further details of convergence problems is left for future research.

5 CONCLUSION

In this paper, we studied the problem of designing the rightmost eigenvalues of a linear scalar system with distributed delay. Our main methodological contributions to spectrum design were the introduction of generalized stability charts and the extension of the Lambert W method to distributed delay systems. Using generalized stability charts we reduced the problem to finding intersections of curves in the parameter plane. In order to characterize design limitations we used numerical continuation. In order to make the matrix Lambert W approach applicable we reformulated the scalar distributed delay system using vector-valued variables and discrete time delays. By exploiting the sparse structure of the appearing matrices we reduced the computation time significantly. We also identified regions in the parameter space where numerical convergence is slow.

Future research work can focus on several extensions. One is

to determine design limitations in higher dimensions [20]. Also, finding more efficient numerical algorithms for the Lambert W method remains an open question. Finally, one may want to better understand the connection between these two approaches.

REFERENCES

[1] Chopra, A. K., 2011. *Dynamics of Structures*, 4th ed. Prentice Hall.

[2] Zuo, L., and Nayfey, S. A., 2004. "Minimax optimization of multi-degree of freedom tuned-mass dampers". *Journal of Sound and Vibration,* **272**(3-5), pp. 893–908.

[3] Bachrathy, D., Insperger, T., and Stépán, G., 2009. "Surface properties of the machined workpiece for helical mills". *Machining Science and Technology,* **13**(2), pp. 227–245.

[4] Dombovári, Z., and Stépán, G., 2012. "The effect of helix angle variation on milling stability". *Journal of Manufacturing Science and Engineering,* **134**(5), p. 051015.

[5] Takács, D., Orosz, G., and Stépán, G., 2009. "Delay effects in shimmy dynamics of wheels with stretched string-like tyres". *European Journal of Mechanics A,* **28**(3), pp. 516–525.

[6] Takács, D., and Stépán, G., 2013. "Contact patch memory of tyres leading to lateral vibrations of four-wheeled vehicles". *Philosophical Transactions of the Royal Society A,* **371**(1993), p. 20120427.

[7] Orosz, G., 2014. "Connected cruise control: modeling, delay effects, and nonlinear behavior". *Vehicle System Dynamics,*(submitted).

[8] Qin, W. B., Gomez, M. M., and Orosz, G., 2014. "Stability analysis of connected cruise control with stochastic delays". In Proceedings of the American Control Conference, no. (accepted).

[9] Duan, S., Ni, J., and Ulsoy, A. G., 2012. "Decay function estimation for linear time delay systems via the Lambert W function". *Journal of Vibration and Control,* **18**(10), pp. 1462–1473.

[10] Breda, D., 2012. "On characteristic roots and stability charts of delay differential equations". *International journal of robust and nonlinear control,* **22**(8), pp. 892–917.

[11] Qiao, W., and Sipahi, R., 2013. "A linear time-invariant consensus dynamics with homogeneous delays: analytical study and synthesis of rightmost eigenvalues". *SIAM Journal on Control and Optimization,* **51**(5), pp. 3971–3992.

[12] Villafuerte, R., Mondie, S., and Garrido, R., 2013. "Tuning of proportional retarded controllers: theory and experiments". *IEEE Transactions on Control Systems Technology,* **21**(3), pp. 983–990.

[13] Insperger, T., 2006. "Act-and-wait concept for continuous-time control systems with feedback delay". *IEEE Transactions on Control Systems and Technology,* **14**(5), pp. 974–977.

[14] Yi, S., Nelson, P. W., and Ulsoy, A. G., 2010. "Eigenvalue assignment for control of time delayed systems using the Lambert W function". *Journal of Vibration and Control,* **16**(7-8), pp. 961–982.

[15] Yi, S., Nelson, P. W., and Ulsoy, A. G., 2010. *Time Delay Systems: Analysis and Control Using the Lambert W Function.* World Scientific.

[16] Lavaei, J., Sojoudi, S., and Murray, R. M., 2010. "Simple delay-based implementation of continuous-time controllers". In Proceedings of the American Control Conference, pp. 5781–5788.

[17] Orosz, G., Moehlis, J., and Murray, R. M., 2010. "Controlling biological networks by time-delayed signals". *Philosophical Transactions of the Royal Society A,* **368**(1911), pp. 439–454.

[18] Bekiaris-Liberis, N., Jankovic, M., and Krstic, M., 2013. "Adaptive stabilization of LTI systems with distributed input delay". *International Journal of Adaptive Control and Signal Processing,* **27**(1-2), pp. 46–65.

[19] Farkas, M., and Stépán, G., 1992. "On perturbation of the kernel in infinite delay systems". *Zeitschrift fur Angewandte Mathematik und Mechanik,* **72**(2), pp. 153–156.

[20] Wei, F., Bachrathy, D., Orosz, G., and Ulsoy, A. G., 2014. "Spectrum design using distributed delay". *International Journal of Dynamics and Control,* **2**(2), pp. 234–246.

[21] Michiels, W., and Niculescu, S.-I., 2007. *Stability and stabilization of time-delay systems. An eigenvalue based approach,* Vol. 12. Advances in Design and Control.

[22] Stépán, G., 1989. *Retarded Dynamical Systems: Stability and Characteristic Functions,* Vol. 210 of *Pitman Research Notes in Mathematics.* Longman.

[23] Åström, K. J., and Murray, R. M., 2008. *Feedback Systems: An Introduction for Scientists and Engineers.* Princeton University Press.

[24] Roose, D., and Szalai, R., 2007. "Continuation and bifurcation analysis of delay differential equations". In Numerical Continuation Methods for Dynamical Systems, B. Krauskopf, H. M. Osinga, and J. Galan-Vioque, eds., Understanding Complex Systems, Springer, pp. 359–399.

[25] Engelborghs, K., Luzyanina, T., and Samaey, G., 2001. DDE-BIFTOOL v. 2.00: a Matlab package for bifurcation analysis of delay differential equations. Tech. Rep. TW-330, Department of Computer Science, Katholieke Universiteit Leuven, Bel-gium. `http://twr.cs.kuleuven.be/research/software/delay/ddebiftool.shtml`.

[26] Yi, S., Duan, S., Nelson, P. W., and Ulsoy, A. G., 2013. "Analysis and control of time delay systems using the LambertWDDE toolbox". In Delay Systems: From Theory to Numerics and Applications, T. Vyhlídal, J.-F. Lafay, and R. Sipahi, eds., Vol. 1 of *Advances in Delays and Dynamics,* Springer, pp. 271–284.

[27] Jarlebring, E., and Damm, T., 2007. "The Lambert W function and the spectrum of some multidimensional time-delay systems". *International Journal of Adaptive Control and Signal Processing,* **43**(12), pp. 2124–2128.

APPENDIX

Consider the matrix $\mathbf{H_k} = \mathbf{A_d Q_k}$ defined in (22). The eigenvalues of $\mathbf{H_k}$ can be obtained from the characteristic equation

$$\det(\lambda \mathbf{I} - \mathbf{H_k}) = \lambda(\lambda + bq_{12}^{\mathbf{k}}) = 0, \tag{25}$$

where $\mathbf{I}$ is the 2-dimensional identity matrix. Using the eigenvectors $\mathbf{v}_1$ and $\mathbf{v}_2$ of $\mathbf{H_k}$ we define the transformation

$$\mathbf{T} = [\, \mathbf{v}_1,\ \mathbf{v}_2 \,], \tag{26}$$

to obtain the Jordan form

$$\mathbf{J_k} = \mathbf{T}^{-1}\mathbf{H_k}\mathbf{T} = \begin{bmatrix} 0 & 0 \\ 0 & -bq_{12}^{\mathbf{k}} \end{bmatrix}. \tag{27}$$

The matrix Lambert W function $\mathbf{W_k}$ for the (vector valued) branch number $\mathbf{k} = [\, k_1,\ k_2 \,]$ can be written as

$$
\begin{aligned}
\mathbf{W_k}(\mathbf{H_k}) &= \mathbf{W_k}(\mathbf{T}\mathbf{J_k}\mathbf{T}^{-1}) \\
&= \mathbf{T}\mathbf{W_k}(\mathbf{J_k})\mathbf{T}^{-1} \\
&= \mathbf{T} \begin{bmatrix} W_{k_1}(0) & 0 \\ 0 & W_{k_2}(-bq_{12}^{\mathbf{k}}) \end{bmatrix} \mathbf{T}^{-1},
\end{aligned} \tag{28}
$$

where the last equality holds for hybrid branches because $\mathbf{J_k}$ is diagonal [15, 27]. Here W_{k_i} is the scalar Lambert W function and it has the property

$$
\begin{cases}
W_{k_i}(0) = 0 & \text{if}\quad k_i = 0, \\
W_{k_i}(0) \to \infty & \text{if}\quad k_i = \pm 1, \pm 2, \dots.
\end{cases} \tag{29}
$$

To avoid singularities we consider the hybrid branches with branch number $\mathbf{k} = [\, 0,\ k \,]$ for $k = 0, \pm 1$ which ensures that we

cover the first two eigenvalues [15]. Then, we have

$$
\begin{aligned}
\mathbf{W_k}(\mathbf{H_k}) &= \mathbf{T} \begin{bmatrix} W_0(0) & 0 \\ 0 & W_k(-bq_{12}^{\mathbf{k}}) \end{bmatrix} \mathbf{T}^{-1} \\
&= \mathbf{T} \begin{bmatrix} 0 & 0 \\ 0 & W_k(-bq_{12}^{\mathbf{k}}) \end{bmatrix} \mathbf{T}^{-1} \\
&= \frac{W_k(-bq_{12}^{\mathbf{k}})}{-bq_{12}^{\mathbf{k}}} \mathbf{T} \begin{bmatrix} 0 & 0 \\ 0 & -bq_{12}^{\mathbf{k}} \end{bmatrix} \mathbf{T}^{-1} \qquad (30) \\
&= \frac{W_k(-bq_{12}^{\mathbf{k}})}{-bq_{12}^{\mathbf{k}}} \mathbf{H_k} \\
&= \begin{bmatrix} 0 & 0 \\ W_k(-bq_{12}^{\mathbf{k}})q_{11}^{\mathbf{k}}/q_{12}^{\mathbf{k}} & W_k(-bq_{12}^{\mathbf{k}}) \end{bmatrix}.
\end{aligned}
$$

This proves (23).